Effect of geometrical configuration of reactor on a ZrP nano-dispersion process using ultrasonic irradiation

Fukunaga, Saki ; Higashi, Sayaka ; Horie, Takafumi ; Sugiyama, Hiroaki ; Kanda, Akihisa ; Hsu, Tong-Yang ; Tung, Kuo-Lun ; Taniya, Keita ;…

(Citation)
Ultrasonics Sonochemistry,52:157-163

(Issue Date)
2019-04

(Resource Type)
journal article

(Version)
Version of Record

(URL)
https://hdl.handle.net/20.500.14094/90008118

Ultrasonics - Sonochemistry 52 (2019) 157–163

Contents lists available at ScienceDirect

Ultrasonics - Sonochemistry

journal homepage: www.elsevier.com/locate/ultson

Effect of geometrical configuration of reactor on a ZrP nano-dispersion process using ultrasonic irradiation

Saki Fukunaga[a], Sayaka Higashi[a], Takafumi Horie[a], Hiroaki Sugiyama[b], Akihisa Kanda[b], Tong-Yang Hsu[c], Kuo-Lun Tung[c], Keita Taniya[a], Satoru Nishiyama[a], Naoto Ohmura[a,*]

[a] Department of Chemical Science and Engineering, Graduate School of Engineering, Kobe University, Japan
[b] Process Technology Laboratories, Kaneka Corporation, Japan
[c] Department of Chemical Engineering, National Taiwan University, Taiwan

ARTICLE INFO

Keywords:
Layered compound
Zirconium phosphate
Fragmentation rate
Geometrical configuration

ABSTRACT

This study investigated the position of ultrasonic irradiation source and reactor geometry on fragmentation rate of a layered compound, α-zirconium phosphate (α-ZrP). By numerically solving the acoustic pressure distribution using COMSOL Multiphysics®, it is clarified the mechanism whereby the operating factors influenced the α-ZrP dispersion to make a suggestion of guideline of the process design method. Two vessels made of glass with a flat-bottom and a spherical-bottom, respectively, were used. Although the flat-bottom vessel at lower horn position showed the best performance of fragmentation, the region of high acoustic pressure field in the flat bottom vessel sharply narrowed and the transmittance became prominently low. On the other hand, no significant difference of the transmittance value in the spherical bottom vessel between the cases of low and high horn positions could be observed and the spherical bottom vessel was robust for the horn position. These results suggest that not only the magnitude of acoustic pressure but also the size of high acoustic pressure region is also an important factor and a spherical bottom vessel is one of suitable shape which gives large size of high acoustic pressure region regardless of the horn position.

1. Introduction

Nano-fillers have received considerable attention since they may lead to enhanced nanocomposites properties with a small amount of filler content [1]. It was reported that the introduction of nano-fillers made of inorganic layered compounds resulted in the improvement of thermal stability [2], mechanical properties [3] and gas barrier properties [4]. Synthetic layered compounds, such as alpha zirconium phosphate (α-ZrP) has attracted attention recently. The α-ZrP has higher ion exchange capacity than montmorillonites [5]. Hence, it is relatively easy to achieve higher degree of exfoliation in ZrP nanoplatelets [6]. In addition, α-ZrP and its derivatives can help improve proton conductivity of certain materials. This allows for the preparation of proton conductive nanocomposites, which can find applications in the fuel [7].

The generation methods of nanomaterials are classified into two approaches *i.e.* a bottom-up approach that atoms agglutinate and become cluster as nanomaterial, and a top-down approach that large particles are fractured and become nanomaterials by adding various energy. Among these two approaches, the top-down approach is considered to be suitable for mass production of nanomaterials because the operation method is relatively simple. In the top-down approach an ultrasonic irradiation method is one of the potential methods to produce nanomaterials. This method has an advantage as compared with the other thermal and mechanical methods; *i.e.* even low power consumption enables to attain high production rate [8]. With this advantage, the ultrasonic irradiation method is one of the promising methods in process intensification. Nagatomo et al. [9] used ultrasonic irradiation for pretreatment of emulsion polymerization of styrene. They successfully showed that the pretreatment of ultrasonic irradiation as short as 1 min drastically improved monomer dispersion and increased reaction rate even under the agitation condition with low rotational speed of impeller.

For mass production of nanomaterials by ultrasonic irradiation method, it is important to construct a model of fragmentation rate, optimize reactor shape and operating conditions. Our previous work [10] proposed an experimental fragmentation equation based on the mass concentration of the α-ZrP, and the experimental results agreed well with the simulation results obtained by the fragmentation rate equation. On the other hand, it is difficult to say that the optimization

* Corresponding author at: 1-1 Rokko-dai, Nada-ku, Kobe 657-8501, Japan.
E-mail address: ohmura@kobe-u.ac.jp (N. Ohmura).

https://doi.org/10.1016/j.ultsonch.2018.11.008
Received 22 April 2018; Received in revised form 25 August 2018; Accepted 9 November 2018
Available online 09 November 2018
1350-4177/

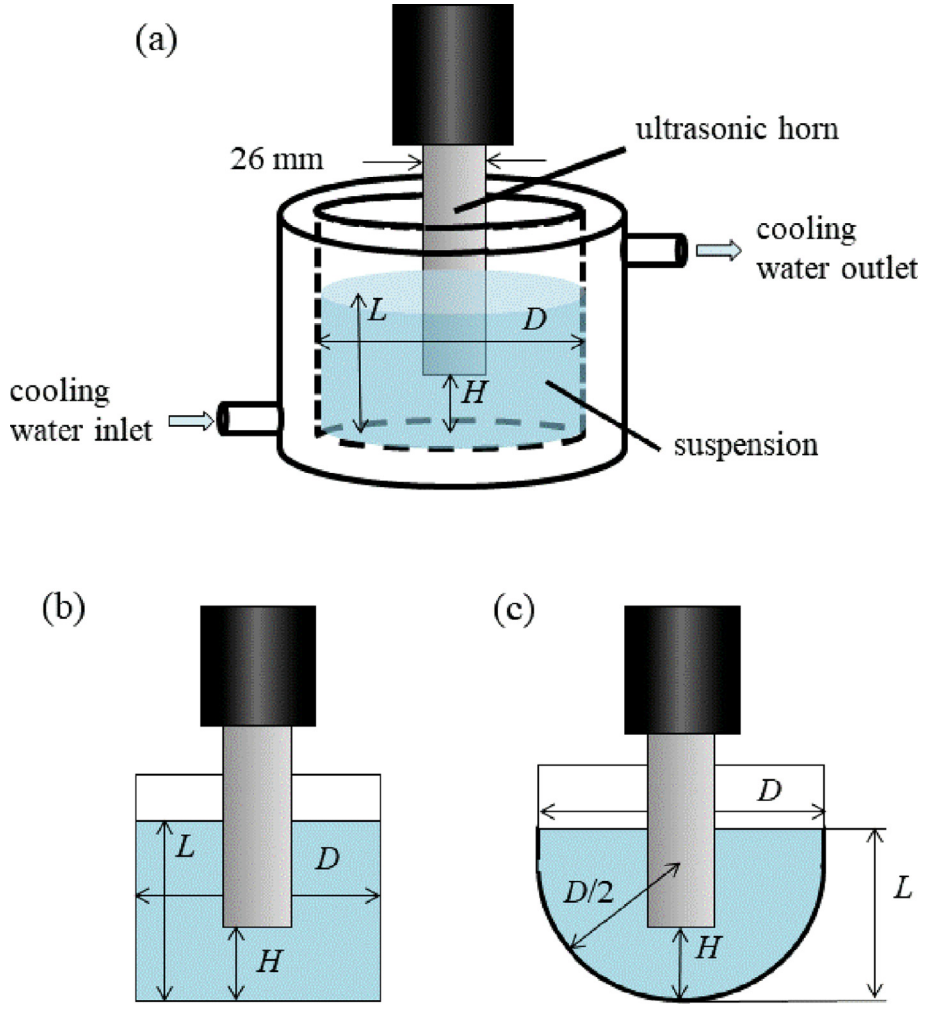

Fig. 1. Schematics of horn-type reactors; (a) flat-bottom vessel with water jacket (D = 70 mm), (b) flat-bottom vessel (D = 100 mm), (c) spherical-bottom vessel (D = 125 mm).

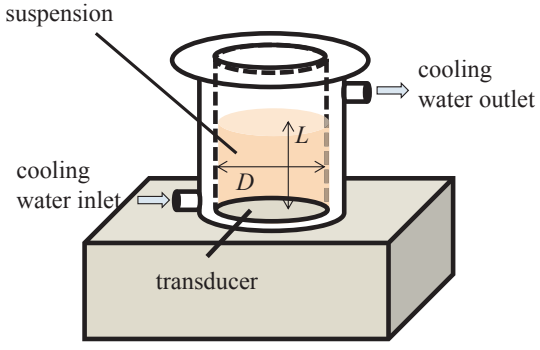

Fig. 2. Schematic of bath-type reactor (D = 53 mm, L = 57 mm).

Table 1
Relation between H and L when using the horn-type reactors; (a) flat-bottom vessel with water jacket, (b) flat-bottom vessel, and (c) spherical-bottom vessel.

(a)				
H [mm]	15	25	40	60
L [mm]	74	72	70	67
(b)				
H [mm]		15		40
L [mm]		68		65
(c)				
H [mm]		15		40
L [mm]		62		61

Table 2
Values of parameters in numerical simulation.

ρ_0	Density [kg/m^3]	998
c_0	Sound velocity [m/s]	1500
f	Ultrasonic frequency [kHz]	20
P_U	Input power [W]	32
r	Radius of transducer [m]	0.013

method of reactor shape and operation conditions has been established yet. In the fragmentation process using ultrasonic irradiation, physical effects due to cavitation play an important role. Cavitation is a very complicated and highly localized phenomenon affected by many factors such as output, frequency, temperature, solution properties [11]. The mechanisms whereby cavitation affects the size and production rate of nanomaterials are still unclear and it is difficult to control the particle size and predict the performance of ultrasonic reactors. This is one of the major restrictions in optimization of ultrasound application in industries [12]. Furthermore, the acoustic field decays rapidly with the propagation distance, and almost all the amount of energy is converted to thermal energy within a small volume near the horn and few cavitation occurs at the region far from the horn. This results in low

Table 3
Density and sound velocity of media.

Medium	Density (kg/m^3)	Sound velocity (m/s)
Water	998	1500
Air	1.2	343
Glass	2500	5100
Ceramics	787.4	5600

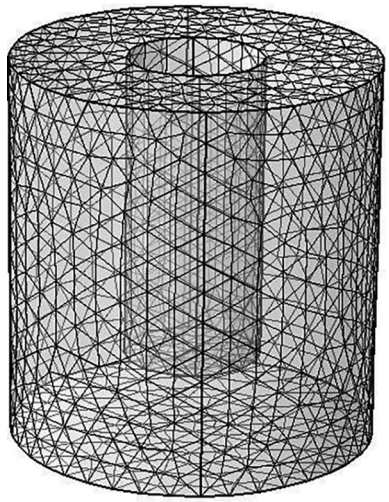

Fig. 3. Mesh for the calculation of acoustic pressure distribution in horn-type reactor.

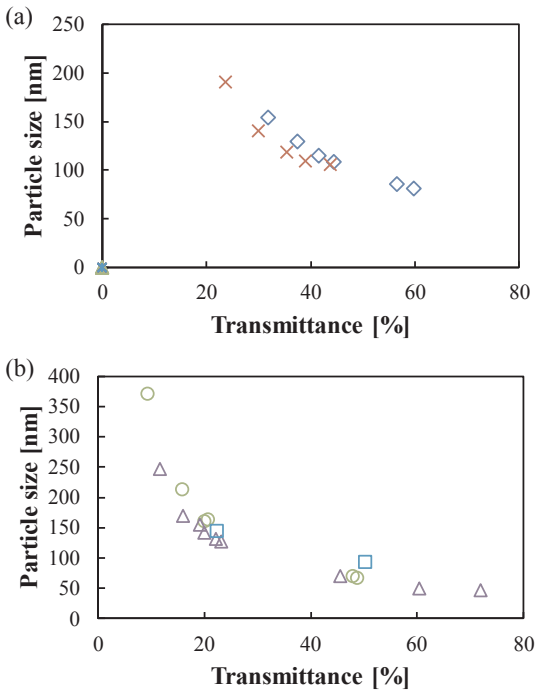

Fig. 4. Correlation between transmittance and mean particle size: (a) Effect of horn position (◊: H = 15 mm, ×: H = 40 mm), and (b) effect of frequency (○ 22 kHz, △ 98 kHz, □ 128 kHz).

efficiency of acoustic energy [13]. Therefore, the scale of a device is limited. In order to solve this problem, it is necessary to intensify the sound pressure field and the cavitation field by optimizing the geometry of the device. If the geometry of reactor is different, it is suggested that the cavitation dynamics would change and that this change would affect the acoustic pressure field and cavitation field. Therefore, in order to achieve intensification of an ultrasonic process by optimization of ultrasonic equipment, it is necessary to elucidate the effects of reactor geometry on ultrasonic efficiency. A numerical approach combined with experiments is one of powerful tools to elucidate these effects. Wei and Weavers [14] used computational simulations using COMSOL Multiphysics® and acoustic pressure maps to design a large-scale sono-reactor containing a multi-stepped ultrasonic horn, and they showed that coupling of COMSOL simulations with hydrophone measurements was a simple, effective and reliable scientific method to evaluate reactor designs of ultrasonic systems. Tiong et al. [15] calculated acoustic pressure fields generated by endosonic files with varying dimensions for the uses of ultrasound in dentistry by the COMSOL simulation package.

This study investigated the position of ultrasonic irradiation source and reactor geometry on fragmentation rate of a layered compound, α-ZrP. By numerically solving the acoustic pressure distribution using COMSOL Multiphysics®, it is clarified the mechanism whereby the operating factors influenced the α-ZrP dispersion to make a suggestion of guideline of the process design method.

2. Materials and methods

α-ZrP particles (molecular weight 301.192 g/mol, particle size 0.5–1.5 μm, Daiichi Kigenso Kagaku Kogyo Co., Ltd.) were dried in air at 120 °C for 3 h as the pretreatment. The α-ZrP suspension (0.25–1.0 wt%) was prepared by mixing α-ZrP particles, distilled water and tetrabutylammonium hydroxide (TBAH) – 40% methanol solution (molecular weight 259.5 g/mol, Lion Specialty Chemicals Co., Ltd.). The mole ratio of α-ZrP to TBAH was 1:1. α-ZrP particles were suspended in the solution. TBAH was used as the compound for intercalation between the α-ZrP layers and swell of the layered structure. Since the dilute solution of ZrP (0.25–1.0 wt%), the properties of the suspension such as speed of sound of the solution, density, viscosity and the acoustic impedance was regarded as the same as water in this study.

The present study used two kinds of reactors, *i.e.* horn-type and bath-type reactors, as shown in Figs. 1 and 2. The diameter of the vessel, the liquid height and the horn position (height from the bottom) was defined as D, L and H, respectively. When the horn-type reactor was used, ultrasonic waves were irradiated directly to the suspension from the tip of the horn-type transducer (US-300T, NIHONSEIKI KAISHA LTD.) with frequency of 20 kHz, which has the maximum electric power output 300 W. Two vessels made of glass with a flat-bottom and a spherical-bottom, respectively, were used. As the horn is deeply inserted, the liquid height increases under the same liquid volume condition. The relationship between H and L is shown in Table 1. Temperature of the α-ZrP suspension in a storage vessel was kept at constant by immersing it in a temperature-controlled bath. The suspension temperature in the flat-bottom vessel was controlled by feeding cooling water of 10 °C by a circulation pump (CCA - 1111, EYELA) into a water jacket attached with the vessel.

On the other hand, in order to investigate the effect of frequency on the fragmentation rate, a bath-type reactor was used as shown in Fig. 2. Ultrasonic waves were irradiated directly to the suspension from the bottom with the transducer having the maximum voltage of 20 Vp-p and the range of frequency from 20 kHz to 30 MHz. The vessel made of stainless steel was the flat-bottom and had a jacket. Cooling water at 20 ± 2 °C was fed into the water jacket by a circulation pump (CTP-1000, EYELA) and the temperature of suspension was kept at constant.

The state of the fragmentation was evaluated by measuring the light transmittance of the suspension (wavelength: 298 nm) with a UV–vis spectrophotometer (MPS-2400, Shimadzu Corporation). The mean particle size was measured by a dynamic light scattering, DLS (ELSZ-0H, Otsuka Electronics Co., Ltd.). The input power of ultrasound P_U [W] was calculated using a calorimetry method which measures the increase of temperature in the system as the ultrasonic power. P_U was calculated

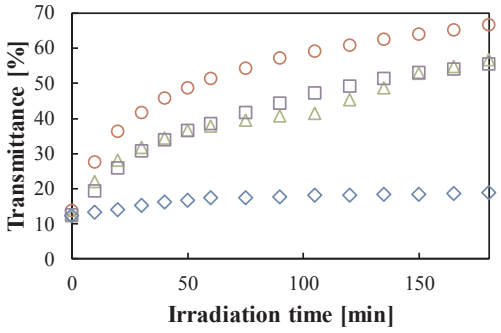

Fig. 5. Effect of frequency on time course change of the transmittance of α-ZrP suspension; ○: 22 kHz, △: 98 kHz, □: 128 kHz ◊: 940 kHz.

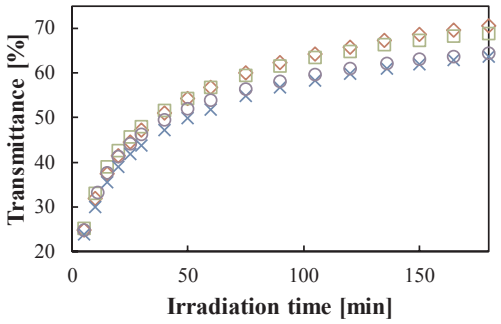

Fig. 6. Effect of horn position on time course change of the transmittance of α-ZrP suspension; ◊: H = 15 mm, □: H = 25 mm, ×: H = 40 mm, ○: H = 60 mm.

with following equation.

$$P_U = wC_P\frac{\Delta T}{\Delta t} \tag{1}$$

w, C_p and $(\Delta T/\Delta t)$ are the water mass, specific heat at a constant pressure of water and the rate of the temperature increase in adiabatic condition, respectively.

When aluminum foil is positioned in the cross section of the vessel and exposed to the ultrasound field, erosion of aluminum can be observed where cavitation is generated. By utilizing this property, the spatial distribution of cavitation in the reactor was observed [16]. The erosion area (cavitation area) [mm^2] of the aluminum foil after 30 s of the ultrasonic irradiation was calculated by Eq. (2).

$$\text{Erosion area} = \text{initial area of cross section} \times \frac{\textit{Weight loss of Aluminum}}{\textit{Initial weight of Aluminum}} \tag{2}$$

3. Numerical simulation of acoustic pressure

Acoustic pressure distribution was calculated by a finite element method software, COMSOL Multiphysics 5.2® (COMSOL AB). The governing equations are as follows:

$$\nabla\cdot\left(\frac{1}{\rho_0}\nabla p\right) - \frac{\omega^2 p}{\rho_0 {c_0}^2} = 0 \tag{3}$$

$$\omega = 2\pi f \tag{4}$$

The symbols and their values of parameters appearing in the above equations are shown in Table 2.

When ultrasound is irradiated to the medium, the medium also vibrates as the acoustic pressure vibrates. At the maximum of the acoustic pressure during the vibration of acoustic pressure, the acceleration of the local area of medium is expressed by the following equation [17].

$$a_n = \omega\sqrt{\frac{2I}{\rho_0 c_0}} \tag{5}$$

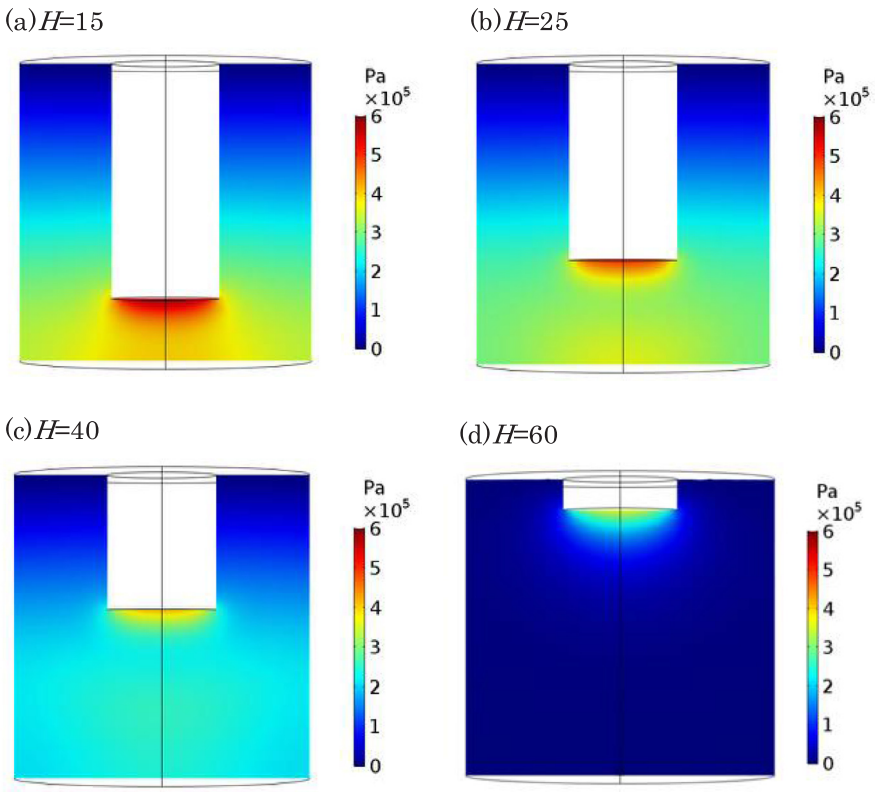

Fig. 7. Acoustic pressure distributions at H = 15, 25, 40 and 60 mm.

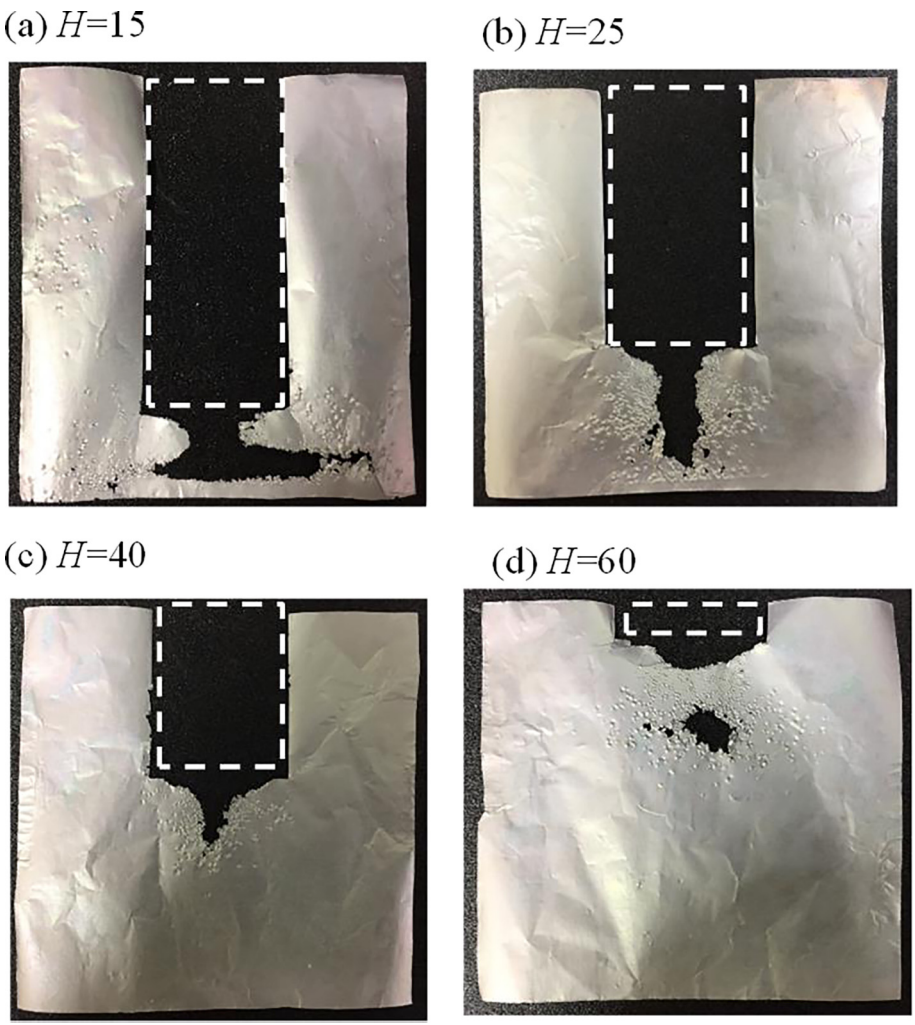

Fig. 8. States of aluminum foil after ultrasonic irradiation for 30 s.

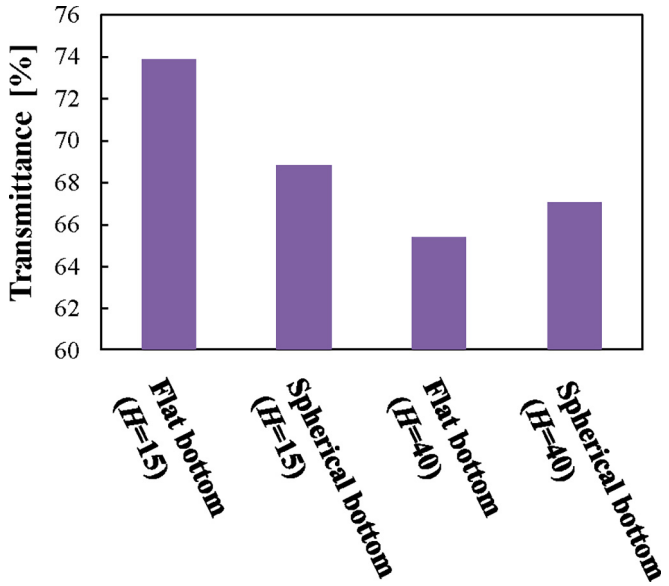

Fig. 9. Transmittance after ultrasonic irradiation for 60 min.

$$I = \frac{P_U}{\pi r^2} \tag{6}$$

This was given as the condition on the cross section of the ultrasonic irradiation source, and the acoustic pressure distribution was calculated. The boundary conditions of acoustic impedance were the same way as Jiao et al. [18]. The impedance boundaries were utilized to specify the boundary conditions of water-air, water-ceramic (horn), water-glass (vessel wall). The density and sound velocity of medium is shown in Table 3. Fig. 3 shows tetrahedral mesh for the calculation of acoustic pressure distribution. The maximum mesh size is 5.92 mm in the horn-type reactor. Sajjadi *et al.* [19] investigated influence of ultrasound power on acoustic streaming and micro-bubbles formations in a low frequency (24 kHz) sono-reactor, and their results showed that the effect of acoustic streaming was not negligible. Their power range was, however, 100–400 W which was much higher than our power range (16–32 W). The present study confirmed that acoustic streaming was very small. Hence the present study did not take the hydrodynamic effects into consideration. In addition, owing that α-ZrP is a nanoparticle, the effect of α-ZrP on fluid flow is negligibly small. It is, therefore, assumed that to be completely miscible and occur as a single-phase slurry.

4. Results and discussion

Prior to the experiments, in order to validate the evaluation of the fragmentation state by the light transmittance of the suspension, the correlation between the mean particle size obtained by DLS and the light transmittance was examined. Fig. 4 shows that the suspension transmittance corresponds to the degree of the fragmentation of nano-

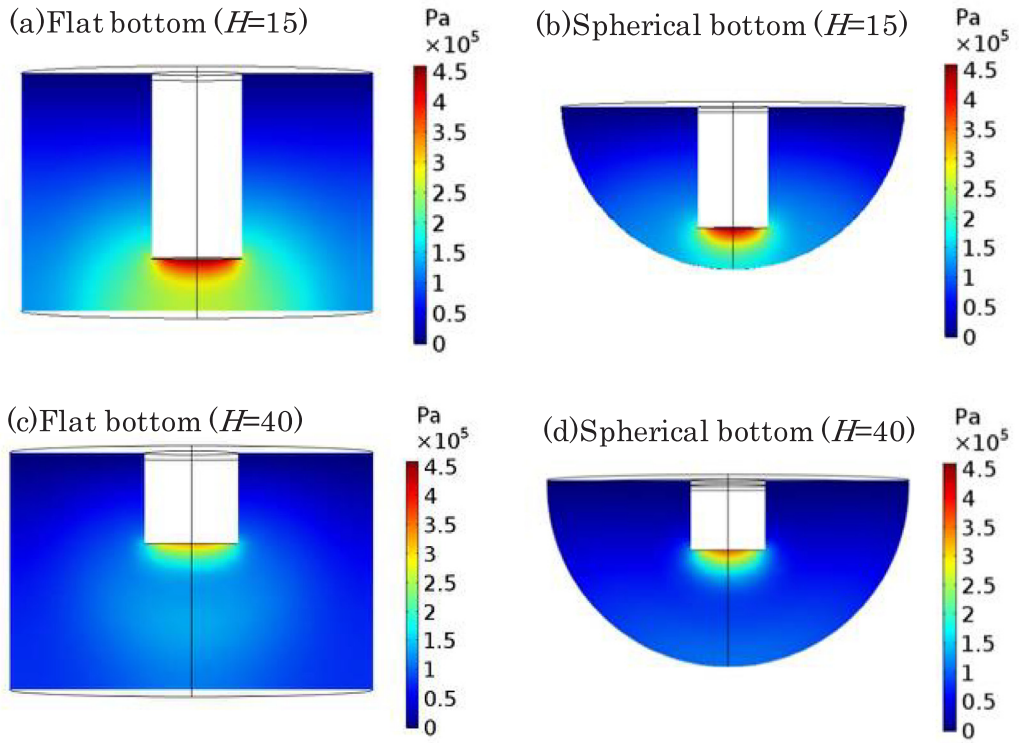

Fig. 10. Acoustic pressure distributions in the flat-bottom and spherical-bottom vessels.

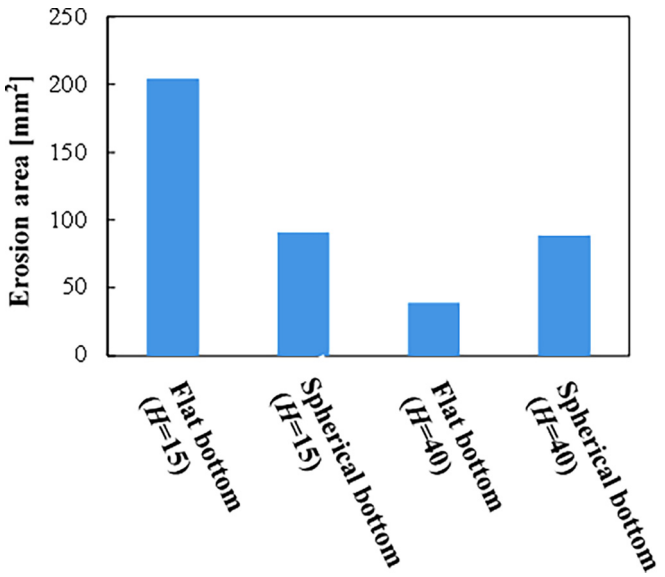

Fig. 11. Erosion area of aluminum foil after ultrasonic irradiation for 30 s.

sized α-ZrP.

In order to verify the validity of conducting the experiments using the horn-type reactor with a fixed frequency of 20 kHz, the effect of frequency on α-ZrP dispersion was investigated by the bath-type device. Driving frequency of ultrasound was varied at 22, 98, 128 and 940 kHz. Concentration of α-ZrP and volume of the suspension were 0.5 wt% and 125 mL, respectively. Ultrasonic energy was 16.0 W. Fig. 5 shows the time course change of the transmittance at various frequencies under sonication. As driving frequency was lower, it showed faster fragmentation rate and higher final transmittance. This result shows the validity of the experiment with the horn type ultrasonic irradiation device with 20 kHz. Hereafter, the effect of geometrical configuration of reactor on the fragmentation rate was investigated by the horn type ultrasonic irradiation device with 20 kHz.

4.1. Effect of horn position

Fig. 6 shows the time course change of the transmittance at various horn positions under sonication. As horn position H was smaller, it showed faster fragmentation rate and higher final transmittance. The result suggested that the smaller H was, the higher shear was exerted to the ZrP particles by cavitation. Moreover, the almost same degree of transmittance was achieved for the sample sonicated for 100 min at $H = 15$ mm and the sample sonicated for 180 min at $H = 40$ mm. It is, therefore, considered that production time can be shortened by about 44.4% by using a reactor with $H = 15$ mm, as compared with $H = 40$ mm.

The acoustic pressure distribution was calculated in order to investigate the magnitude of the acoustic pressure at each horn position, as shown in Fig. 7. The result also indicates that the smaller H was, the higher the maximum value of acoustic pressure was. The rapid attenuation of the acoustic pressure field results in low efficiency of acoustic energy [13]. It is, therefore, suggested that when H becomes small, the maximum value of acoustic pressure increases because of the remarkable interaction without prominent energy loss between the ultrasonic wave irradiated from the horn and the ultrasonic wave reflected on the bottom of the reactor at just below the horn. Fig. 8 shows images of aluminum foil after ultrasonic irradiation for 30 s at each horn position. These images are very similar to the acoustic pressure distribution shown in Fig. 7, and it can be seen that cavitation occurs conspicuously in a place where the magnitude of acoustic pressure is large.

The dead zone in which cavitation is not achieved is one of the most important parameters to consider when using a horn-type sonication [20,21]. These literatures recommend that it is of paramount importance to maintain the distance between the horn tip and the wall container. In the flat bottom case, the dead zone effect ultrasonic

performance is significant.

4.2. Effect of vessel shape

Fig. 9 shows the transmittance values at 60 min irradiation in the flat bottom and spherical bottom vessels with the horn position on $H = 15$ and 40 mm under sonication. Although the flat bottom vessel shows the largest transmittance at $H = 15$ mm, it shows the lowest value at $H = 40$ mm. This indicates that the performance of fragmentation in the flat bottom vessel largely depends on the horn position. On the other hand, no significant difference of the transmittance value in the spherical bottom vessel between the cases of $H = 15$ and 40 mm can be observed. This indicates that the performance of fragmentation in the spherical bottom vessel less depends on the horn position. Fig. 10 shows the acoustic pressure distributions obtained by numerical simulations. Although no significant difference of maximum acoustic pressure between the two kinds of vessels can be seen at each $H = 15$ or 40 mm, the region of high acoustic pressure field in the flat bottom vessel sharply narrows when $H = 40$ mm. On the other hand, the size of high acoustic pressure region around the tip of the horn is still maintained in the spherical bottom vessel. Fig. 11 shows the erosion area calculated by Eq. (2). This figure shows the similar trend to the above discussion. These results suggest that the performance of the spherical bottom vessel is almost independent of the horn position.

As described in the previous section, the ultrasonic intensity rapidly attenuates not only axially but also radially from the tip of horn. When using the spherical bottom, the distance between the tip of horn and the spherical bottom wall does not significantly change as compared with the case of flat bottom. This indicates that the spherical bottom prevents from increasing the dead zone due to rapid attenuation of ultrasonic intensity. Capelo et al. [20] also examined the effect of sampling container shape for chemical analysis on the performance of solid-liquid extraction. They revealed that three eppendorf-type containers which have conical, fan-shape and spherical bottoms, respectively showed appropriate achievement of total extractions, whereas a container having flat bottom showed the lowest efficiency. They also considered that this low efficiency might be the results of the dead cavitation zone. It can be, therefore, considered that a spherical bottom vessel is one of suitable shape which gives large size of high acoustic pressure region regardless of the horn position.

5. Conclusion

This study investigated the effects of the position of ultrasonic irradiation source and reactor geometry on fragmentation rate of a layered compound, α-ZrP. As expected, the closer the horn position to the bottom, the larger the maximum acoustic pressure, due to the reflection of acoustic waves from the bottom. The larger acoustic pressure field gave higher fragmentation rate and higher transmittance. Although the flat bottom vessel at $H = 15$ mm showed the best performance of fragmentation, the region of high acoustic pressure field in the flat bottom vessel sharply narrowed and the transmittance was the lowest when $H = 40$ mm. On the other hand, no significant difference of the transmittance value in the spherical bottom vessel between the cases of $H = 15$ and 40 mm could be observed and the spherical bottom vessel was robust for the horn position. These results suggest that not only the magnitude of acoustic pressure but also the extend of high acoustic pressure region is also an important factor and a spherical bottom vessel is one of suitable shape which gives large size of high acoustic pressure region regardless of the horn position. The results shows that α-ZrP nano-dispersion process can be one of the estimation methods of quantitative determination of the amount of kinetic parameter by the cavitation bubbles.

Acknowledgments

The authors wish to thank Mr. Norihisa Kumagai for his experimental support.

References

[1] K. Dal Pont, J.F. Gérard, E. Espuche, Modification of α-ZrP nanofillers by amines of different chain length: consequences on the morphology and mechanical properties of styrene butadiene rubber based nanocomposites, Eur. Polym. J. 48 (2012) 217–227.
[2] Y. Du, F. Deng, X. Jiang, H. Ji, D. Yu, W. Wang, B. Sun, M. Zhua, Preparation and performance of lipophilic α-zirconium phosphate with high thermal stability and its application in thermal-plastic polymers, Progr. Nat. Sci. Mater. Int. 25 (2015) 503–511.
[3] W.J. Boo, L.Y. Sun, J. Liu, A. Clearfield, H.-J. Sue, M.J. Mullins, H. Pham, Morphology and mechanical behavior of exfoliated epoxy/a-zirconium phosphate nanocomposites, Compos. Sci. Technol. 67 (2007) 262–269.
[4] L. Sun, W.-J. Boo, A. Clearfield, H.-J. Sue, H.Q. Pham, Barrier properties of model epoxy nanocomposites, J. Mem. Sci. 318 (2008) 129–136.
[5] A. Clearfield, W.L. Duax, J.M. Garces, A.S. Medina, On the mechanism of ion exchange in crystalline zirconium phosphates – IV Potassium ion exchange of α-zirconium phosphate, J. Inorg. Nucl. Chem. 34 (1972) 329–337.
[6] L. Sun, W.-J. Boo, R.L. Browning, H.-J. Sue, A. Clearfield, Effect of crystallinity on the intercalation of monoamine in α-zirconium phosphate layer structure, Chem. Mater. 17 (2005) 5606–5609.
[7] L. Sun, J.Y. O'Reilly, D. Kong, J.-Y. Su, W.-J. Boo, H.-J. Sue, A. Clearfield, The effect of guest molecular architecture and host crystallinity upon the mechanism of the intercalation reaction, J. Colloid Interface Sci. 333 (2009) 503–509.
[8] A.N. Nguyen, L. Reinert, J.M. Lévêque, A. Beziat, P. Dehaudt, J.F. Juliaa, L. Duclaux, Preparation and characterization of micron and submicron-sized vermiculite powder by ultrasonic irradiation, Appl. Clay Sci. 72 (2013) 9–17.
[9] D. Nagatomo, T. Horie, C. Hongo, N. Ohmura, Effect of ultrasonic pretreatment on emulsion polymerization of styrene, Ultrason. Sonochem. 31 (2016) 337–341.
[10] T. Horie, S. Akao, T. Suzuki, K. Tanaka, N. Jia, K. Taniya, S. Nishiyama, N. Ohmura, Process development for ultrasonic fracturing of zirconium phosphate particles, J. Chem. Eng. Japan 47 (2014) 124–129.
[11] Y. Kojima, Y. Asakura, G. Sugiyama, S. Koda, The effects of acoustic flow and mechanical flow on the sonochemical efficiency in a rectangular sonochemical reactor, Ultrason. Sonochem. 17 (2010) 978–984.
[12] J. Frohly, S. Labouret, C. Bruneel, I. Looten-Baquet, R. Torguet, Ultrasonic cavitation monitoring by acoustic noise power measurement, J. Acoust. Soc. Am. 108 (2000) 2012.
[13] W. Zhai, H.M. Liu, Z.Y. Hong, W.J. Xie, B. Wei, A numerical simulation of acoustic field within liquids subject to three orthogonal ultrasounds, Ultrason. Sonochem. 34 (2017) 130–135.
[14] Z. Wei, L.K. Weavers, Combining COMSOL modeling with acoustic pressure maps to design sono-reactors, Ultrason. Sonochem. 31 (2016) 490–498.
[15] T.J. Tiong, G.J. Price, S. Kanagasingam, A computational simulation study on the acoustic pressure generated by a dental endosonic file: effects of intensity, file shape and volume, Ultrason. Sonochem. 21 (2014) 1858–1865.
[16] A. Brotchie, F. Grieser, M.A. Ashokkumar, Effect of power and frequency on bubble-size distributions in acoustic cavitation, Phys. Rev. Lett. 102 (2009) 084302.
[17] L. Liu, Y. Yang, P. Liu, W. Tan, The influence of air content in water on ultrasonic cavitation field, Ultrason. Sonochem. 21 (2014) 566–571.
[18] Q. Jiao, X. Bayanhesig, J. Tan, Zhu, Numerical simulation of ultrasonic enhancement on mass transfer in liquid-solid reaction by a new computational model, Ultrason. Sonochem. 21 (2014) 535–541.
[19] B. Sajjadi, A.A.A. Raman, S. Ibrahim, Influence of ultrasound power on acoustic streaming and micro-bubbles formations in a low frequency sono-reactor: mathematical and 3D computational simulation, Ultrason. Sonochem. 24 (2015) 193–203.
[20] J.L. Capelo, M.M. Galesio, G.M. Felisberto, C. Vaz, J. Costa Pessoa, Micro-focused ultrasonic solid-liquid extraction (μFUSLE) combined with HPLC and fluorescence detection for PAHs determination in sediments: optimization and linking with the analytical minimalism concept, Talanta 66 (2005) 1272–1280.
[21] H.M. Santos, C. Lodeiro, J.-L. Capelo-Martinez, The power of ultrasound, in: J.-L. Capwlo-Martinez (Ed.), Ultrasound in Chemistry, WILEY-VCH Verlag GmbH& Co.KGaA, Weinheim, Germany, 2009, pp. 1–16.